

Beyond single tetrahedron physics of the breathing pyrochlore compound $\text{Ba}_3\text{Yb}_2\text{Zn}_5\text{O}_{11}$

Rabindranath Bag ^{1,*}, Sachith E. Dissanayake^{1,*}, Han Yan^{2,3}, Zhenzhong Shi¹, David Graf⁴, Eun Sang Choi⁴, Casey Marjerrison¹, Franz Lang ⁵, Tom Lancaster ⁶, Yiming Qiu⁷, Wangchun Chen ⁷, Stephen J. Blundell ⁵,
Andriy H. Nevidomskyy ² and Sara Haravifard ^{1,8,†}

¹*Department of Physics, Duke University, Durham, North Carolina 27708, USA*

²*Department of Physics and Astronomy, Rice University, Houston, Texas 77005, USA*

³*Rice Academy of Fellows, Rice University, Houston, Texas 77005, USA*

⁴*National High Magnetic Field Laboratory and Department of Physics, Florida State University, Tallahassee, Florida 32310, USA*

⁵*Clarendon Laboratory & Physics Department, University of Oxford, Parks Road, Oxford OX1 3PU, United Kingdom*

⁶*Department of Physics, Centre for Materials Physics, Durham University, Durham DH1 3LE, United Kingdom*

⁷*NIST Center for Neutron Research, National Institute of Standards and Technology, Gaithersburg, Maryland 20899, USA*

⁸*Department of Materials Sciences and Mechanical Engineering, Duke University, Durham, North Carolina 27708, USA*



(Received 12 October 2022; revised 6 February 2023; accepted 5 April 2023; published 20 April 2023)

Recently, a new class of quantum magnets, the so-called breathing pyrochlore spin systems, have attracted much attention due to their potential to host exotic emergent phenomena. Here, we present magnetometry, heat capacity, thermal conductivity, muon-spin relaxation, and polarized inelastic neutron scattering measurements performed on high-quality single crystal samples of the breathing pyrochlore compound $\text{Ba}_3\text{Yb}_2\text{Zn}_5\text{O}_{11}$. We interpret these results using a simplified toy model and provide insight into the low-energy physics of this system beyond the single tetrahedron physics proposed previously.

DOI: [10.1103/PhysRevB.107.L140408](https://doi.org/10.1103/PhysRevB.107.L140408)

Frustrated quantum magnets provide a fruitful arena to search for novel quantum phenomena [1,2]. Pyrochlore lattice magnets, in which magnetic ions form corner-sharing regular tetrahedra, are one of the most studied frustrated systems in three dimensions [3–6]. In the pyrochlore system the conventional magnetic ordering is suppressed by the geometrically frustrated lattice, consequently resulting in emergence of exotic phases [7–19]. Recently, a new class of systems, the so-called breathing pyrochlore magnets, have attracted much attention due to their potential to host exotic phenomena and topological phases [20–23]. In breathing pyrochlore compounds the lattice inversion symmetry at each site is broken due to the different sizes of up-pointing and down-pointing tetrahedra, thus resulting in large Dzyaloshinskii-Moriya (DM) interactions on the two tetrahedra [24] [see Figs. 1(a) and 1(b) for the structure of breathing pyrochlores]. On the theory front, recent works have shown that breathing pyrochlore spin systems can host novel physics including classical rank-2 $U(1)$ spin-liquid states [25], quantum fractons [26], competing quantum spin liquids [27], and hedgehog lattices of magnetic monopoles and antimonopoles [23]. Thus it is of great interest to synthesize and understand breathing pyrochlore materials. The majority of the work performed on the breathing pyrochlore-based compounds has focused on Cr-based spinels with $S = 3/2$ [28–36], while the studies performed on quantum systems with $S = 1/2$ remain limited to $\text{Ba}_3\text{Yb}_2\text{Zn}_5\text{O}_{11}$ in powder form [37–42].

We successfully grew single crystal samples of the breathing pyrochlore $\text{Ba}_3\text{Yb}_2\text{Zn}_5\text{O}_{11}$ using the modified optical floating zone technique. Inelastic neutron scattering studies using our single crystal sample revealed that the single tetrahedron model with isolated tetrahedra can explain the high-temperature and high-energy regime of the collected data. However, the diffuse neutron scattering performed at low temperature and low energy reveals features which cannot be understood with this model [43]. Pair distribution function (PDF) analyses performed on high-quality powder neutron diffraction data provided evidence for the absence of chemical disorder within experimental resolution. Single crystal x-ray diffraction studies also found no evidence of site disorder, ruling out the previously proposed explanations to describe the low-temperature heat capacity results obtained for powder samples of $\text{Ba}_3\text{Yb}_2\text{Zn}_5\text{O}_{11}$ [39,42]. This calls for additional experimental and theoretical efforts to provide us a better understanding of the physics governing magnetic properties of $\text{Ba}_3\text{Yb}_2\text{Zn}_5\text{O}_{11}$ and possibly similar breathing pyrochlore systems.

In this Research Letter, we report low-temperature heat capacity measurements in applied field and ultrasensitive magnetic susceptibility, thermal conductivity, muon spin relaxation (μ^+ SR), and polarized inelastic neutron scattering measurements of the ytterbium-based breathing pyrochlore compound $\text{Ba}_3\text{Yb}_2\text{Zn}_5\text{O}_{11}$ in single crystalline form, to investigate the intrinsic low-temperature magnetic properties and provide a first look into the physics governing the low-energy regime of this system. We propose a simplified model that captures the field dependence of the heat capacity for the lower-field region well and provides a scenario beyond

*These authors contributed equally to this work.

†sara.haravifard@duke.edu

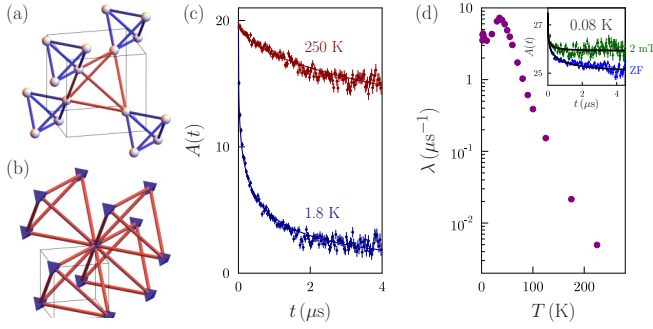


FIG. 1. (a) Structure of the breathing pyrochlore lattice. Considering each A tetrahedron (blue) as a single site and retaining the bonds on the B tetrahedron (red), we obtain a face-centered cubic (fcc) lattice shown in (b). The cube shown with solid black lines marks the repeating unit in the left panel in the fcc lattice. (c) Zero-field muon asymmetry for two temperatures. Solid lines represent fits to $A(t) = A(0)e^{-(\lambda t)^\beta}$ with $A(0)$ fixed across all temperatures. (d) The temperature dependence of the fitted relaxation rate λ . The inset shows ultralow-temperature data, demonstrating the absence of long-range order at 0.08 K and the effect of applying a small 2 mT longitudinal field versus zero field (ZF).

the previously reported single tetrahedron physics, with finite intertetrahedron coupling necessary to interpret the experimental results.

In order to search for any trace of magnetic order, we performed μ^+ SR measurements using a large powder sample of $\text{Ba}_3\text{Yb}_2\text{Zn}_5\text{O}_{11}$ on the General Purpose Surface-Muon Instrument (GPS) spectrometer at the Swiss Muon Source at the Paul Scherrer Institute (PSI) and also using coaligned single crystal samples of $\text{Ba}_3\text{Yb}_2\text{Zn}_5\text{O}_{11}$ mounted in a dilution refrigerator at the MuSR spectrometer of the ISIS Neutron and Muon Source. To understand the origin of the

contributions to the μ^+ SR signal, we carried out density functional theory (DFT) calculations to locate the most probable muon stopping sites and assess the degree of perturbation the muon probe causes in the material [44], which we find to be small in this system (for details, see Supplemental Material [45]). Our μ^+ SR results collected at millikelvin temperatures demonstrate no oscillatory signal, indicating the absence of long-range magnetic ordering in this system. Our ultralow-temperature thermodynamics and neutron diffraction results [43] further confirm the absence of long-range magnetic ordering in $\text{Ba}_3\text{Yb}_2\text{Zn}_5\text{O}_{11}$.

We show in Figs. 2(a)–2(c) and 2(e)–2(i) the magnetic heat capacity for a $\text{Ba}_3\text{Yb}_2\text{Zn}_5\text{O}_{11}$ single crystal sample from 54 mK to 1 K under different applied magnetic fields, with the phonon contribution subtracted using the results of measurements made on isostructural, nonmagnetic $\text{Ba}_3\text{Lu}_2\text{Zn}_5\text{O}_{11}$. The magnetic entropy at zero field is shown in Fig. 2(d). The heat capacity data were collected on two different $\text{Ba}_3\text{Yb}_2\text{Zn}_5\text{O}_{11}$ single crystal samples (grown using different techniques) and are compared with the reported powder $\text{Ba}_3\text{Yb}_2\text{Zn}_5\text{O}_{11}$ sample [45]. Previous reports discussed the possibility of having defects, such as structural disorder, as an underlying cause for the peak observed at low temperatures, whereas our heat capacity data collected on multiple single crystal samples exclude the existence of measurable defect effects such as structural disorder. To further elaborate on this, we show in Fig. S1 of the Supplemental Material [45] the results obtained for two single crystal samples grown with different techniques (sample 1 and sample 2). The peak position at 110 mK remains the same for both single crystal samples and agrees with the reported powder study by Haku *et al.* [39]. This is while the fits to the data are significantly improved using the model we employed to analyze the results. We explain the details of this model in the following. Additionally, here we show the field dependence of the low-temperature

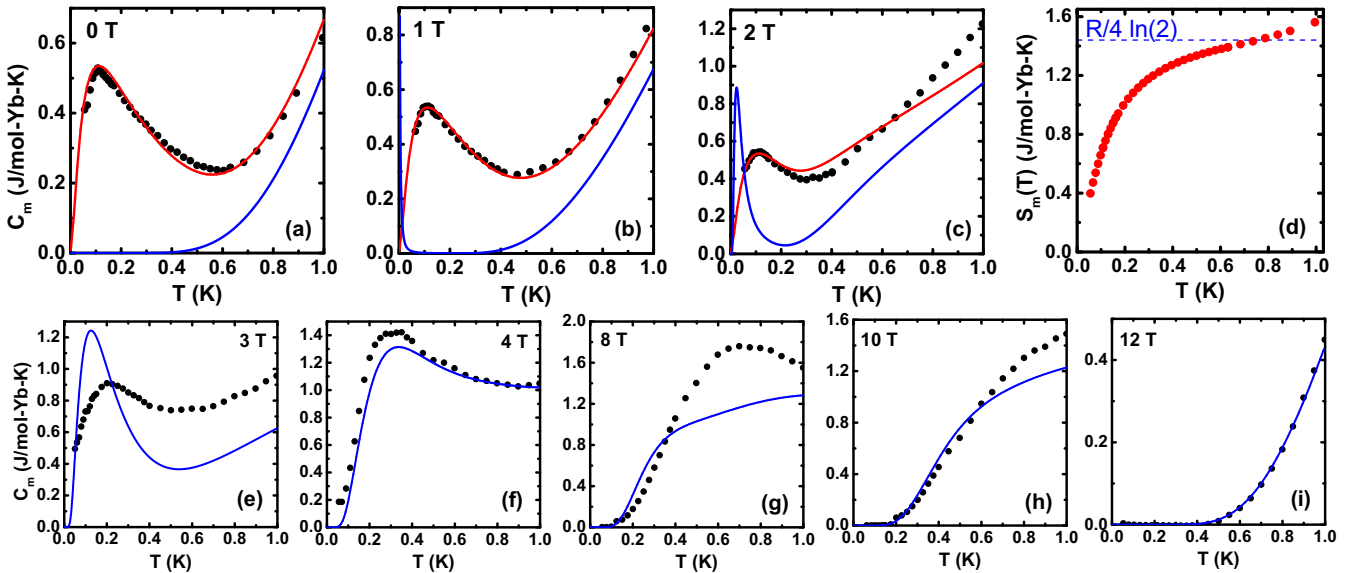


FIG. 2. (a)–(c) and (e)–(i) Low-temperature magnetic specific heat C_m of $\text{Ba}_3\text{Yb}_2\text{Zn}_5\text{O}_{11}$ single crystal samples for different fields from 0 to 12 T. The phonon contribution was subtracted using the isostructural, nonmagnetic compound $\text{Ba}_3\text{Lu}_2\text{Zn}_5\text{O}_{11}$. Red lines are fits based on the effective model on the fcc lattice outlined in the text [45]. Blue lines are obtained from single tetrahedron theory. (d) Magnetic entropy of $\text{Ba}_3\text{Yb}_2\text{Zn}_5\text{O}_{11}$ at zero magnetic field.

feature which agrees reasonably with our proposed model, in particular for the low- and high-field regions.

As shown in Fig. 2(d), there is $\frac{1}{4}R\ln 2$ entropy release per Yb ion, corresponding to an effective pseudospin-1/2 degree of freedom on each tetrahedron. As discussed by Rau *et al.* [42] the experimental specific heat results collected at $T < 0.4$ K disagree with the single tetrahedron model, leading us to propose that this release of entropy is related to the intertetrahedron interactions. This is because in the single tetrahedron theory, the two lowest states are robustly degenerate, and the third state lies much higher in energy (at ~ 0.5 meV). Although for a finite external magnetic field, the degeneracy of the two lowest states is expected to be lifted, the energy splitting is much smaller than ~ 0.01 meV, which cannot explain the broad peak in heat capacity measurement in Figs. 2(a) and 2(b).

The above observations suggest that the low-energy properties of $\text{Ba}_3\text{Yb}_2\text{Zn}_5\text{O}_{11}$ cannot be explained by the single tetrahedron theory, even if tuning the exchange parameters is allowed. Instead, the specific heat data can be understood quantitatively by introducing intertetrahedron interactions. To this end, we have constructed an effective low-energy model, regarding the two nearly degenerate lowest energy states (out of 16) on the A tetrahedra as a pseudospin 1/2. This is justified by the fact that the other states lie at much higher energies ($E_3 > 0.3$ meV) [42] relative to the range $T < 1$ K in our specific heat data.

From exact diagonalization on a single tetrahedron, we can determine the wave function of the two lowest states exactly, which form the two-dimensional (E) irreducible representation of the T_d point group. In the limit of vanishing intratetrahedron DM interaction, these states span the two-dimensional Hilbert space of two-dimer coverings of the four sites. Note that there are three such possible dimer coverings classically, but one of them is linearly dependent on the other two. The small DM interaction in A tetrahedra tunes the wave function away from the perfect dimer-covering states [38,46] but does not lift their degeneracy, justifying our treating them as pseudospin-1/2 degrees of freedom. We then consider the interaction between these pseudospins via the weak bonds on the B tetrahedra [shown in red in Figs. 1(a) and 1(b)]. Shrinking every A tetrahedron to a point connected by these weak bonds, the effective low-energy model becomes a face-centered cubic (fcc) lattice of pseudospins with nearest-neighbor interactions [cf. Fig. 1(b)]. The effective interactions are the original interactions between the physical spins projected onto the pseudospin Hilbert space.

We consider the simplest model of the effective interactions between neighboring A -tetrahedra pseudospins:

$$H = J_{xy}(s_i^x s_j^x + s_i^y s_j^y) + J_z s_i^z s_j^z. \quad (1)$$

We find that choosing ferromagnetic $J_z = -0.005$ meV and antiferromagnetic $J_{xy} = 0.0125$ meV in this XXZ model can reproduce the zero-field specific heat very well [Fig. 2(a)] (for details, see Supplemental Material [45]). The origin of the 110-mK peak in the specific heat is due to buildup of ferromagnetic correlations of the pseudospins, which spontaneously lifts the twofold degeneracy of the single tetrahedron model. Linear spin-wave theory then produces pseudomagnons of the bandwidth $\sim J_{xy}$ which propagate on

the fcc lattice, as depicted in Fig. S4 [45]. It is important to note that pseudomagnons are not conventional spin waves, but rather collective excitations of the dimer-covering states spanned by pseudospin degrees of freedom on A tetrahedra, and hence may be challenging to detect by inelastic neutron scattering.

The effective low-energy model in Eq. (1) is expected to work in a moderately large applied magnetic field, provided its strength does not exceed the energy gap ($E_3 \sim 0.38$ meV) to the first excited state beyond the E doublet in the single tetrahedron model [42]. The magnetic field splits pseudospin degrees of freedom in Eq. (1) at an energy scale much smaller than the parameters in the effective model (Fig. S3 in the Supplemental Material [45]). The main effect of the field, from the exact diagonalization of a single tetrahedron, is to shift the higher-energy states downwards, which we treat as flat bands. This approximation breaks down at a critical value of the field $B_c \sim 4$ T when the lowest excited state E_3 crosses the ground-state doublet, resulting in a phase transition. Our model (1) does not apply in this regime or higher fields. In the limit of high fields $B > 10$ T, we are able to obtain a good match with the experimental specific heat [see Fig. 2(i)] by using a single tetrahedron theory, which predicts a unique nondegenerate ground state separated by a large gap from the higher-lying states. For intermediate field strengths, one cannot ignore the effect of the excited states, which result in the ground-state level crossing as already noted. The minimal model then becomes rather complicated, with a vast range of unknown parameters, whose determination lies beyond the scope of the present work.

Further insight into the effect of weak magnetic fields can be gleaned from the magnetic ac susceptibility, which we measured on two separate $\text{Ba}_3\text{Yb}_2\text{Zn}_5\text{O}_{11}$ crystals. The results are shown in Fig. 3(a), which show two anomalies at $\mu_0 H_{c1} = 0.32$ T and $\mu_0 H_{c2} = 1.0$ T upon cooling at low temperatures $T \simeq 0.3$ K. The two anomalies are also seen in the tunnel diode oscillator (TDO) measurements on the same crystals and do not shift appreciably with field when the crystal is rotated away from the [111] orientation [see Fig. 3(b)]. These anomalies are independent of two different oscillation frequencies (1616 and 87.1 Hz) of the ac-susceptibility measurement, suggesting the signal is unrelated to spin freezing and consistent with the μ^+ SR study showing absence thereof. The most likely explanation for the anomalies is the level crossing at the corresponding fields $\mu_0 H_{c1}$ and $\mu_0 H_{c2}$. Given the high frustration of the fcc lattice, it is possible for the system to go through several different phases. The exact phases and phase transitions cannot be determined by current experimental data and await future effort. Importantly, the explanation must involve intertetrahedron couplings, because the single tetrahedron model would predict a nonmagnetic $S_{\text{eff}} = 0$ ground state at low temperatures (≤ 0.5 K) and thus a featureless magnetic susceptibility, contrary to what we see in our measurements.

In order to further understand the nature of the low-lying states observed in the heat capacity and magnetometry data, low-temperature thermal conductivity measurements were carried out on single crystal samples of $\text{Ba}_3\text{Yb}_2\text{Zn}_5\text{O}_{11}$ [45]. A power-law fit ($\kappa_{xx} \sim T^\alpha$) is performed on the collected data in the high- T region, and the value of the exponent

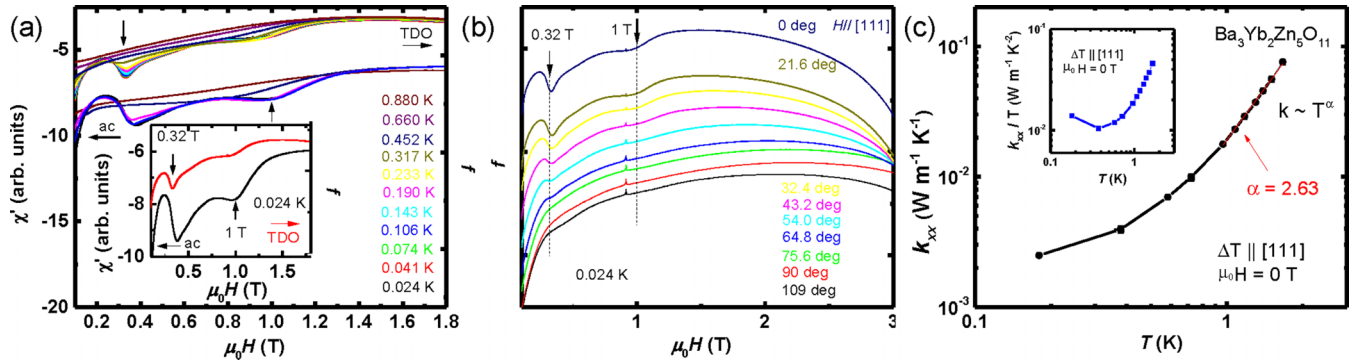


FIG. 3. Low- H anomalies beyond the single tetrahedra model: (a) magnetic ac susceptibility χ' (left axis) and TDO frequency f (right axis) as a function of external magnetic field ($H \parallel [111]$) at different temperatures. Two anomalies are marked by arrows. χ' is measured with an oscillating frequency of 1616 Hz. Measurements (χ') with different frequency (87.1 Hz) reproduce the two anomalies at the same fields. The inset shows a zoomed-in plot of χ' (left axis) and TDO f (right axis) at $T = 0.024$ K. (b) TDO frequency f data are shown for different rotation angles between the field and the crystal $[111]$ axis at 0.024 K. Traces are shifted vertically for clarity. Note that the sharp feature seen just below 1 T field originates from the nuclear magnetic resonance (NMR) signal of hydrogen (mainly in solvents of silver paint used to mount the sample). (c) Thermal conductivity data (κ_{xx} vs T) for $\text{Ba}_3\text{Yb}_2\text{Zn}_5\text{O}_{11}$ at $\mu_0 H = 0$ T; $\delta T \parallel [111]$. The solid red line is a power-law fit to the κ_{xx} data. A clear saturation of κ_{xx} at low T is seen for $\text{Ba}_3\text{Yb}_2\text{Zn}_5\text{O}_{11}$. The inset shows a κ_{xx}/T vs T plot.

(α) is found to be 2.63. For a nonmagnetic insulator, κ_{xx} at very low temperature is only due to the contribution from phonons [47,48]. However, the exponent value obtained for $\text{Ba}_3\text{Yb}_2\text{Zn}_5\text{O}_{11}$ reveals additional contributions coming from various quasiparticles such as phonons, spinons, and magnons, as well as different scattering channels for the heat current [48–51]. Interestingly, at low T , a clear saturation of κ_{xx} in $\text{Ba}_3\text{Yb}_2\text{Zn}_5\text{O}_{11}$ is seen. Such saturation is not expected in conventional magnets, where both phonons and magnons freeze-out, but suggests itinerant fermionic (spinon) excitations expected in gapless spin-liquid candidates [47,51–53]. Further studies are needed to probe the nature of these low- T magnetic excitations. To provide a better understanding of the underlying physics governing the physics of $\text{Ba}_3\text{Yb}_2\text{Zn}_5\text{O}_{11}$ at ultralow temperatures, we have complemented these efforts by performing polarized inelastic neutron scattering measurements on single crystal samples (for details, see Supplemental Material [45]). The results of this experiment are shown in Figs. 4(a) and 4(b), in which $T = 0.1$ K and $E = 0.5$ meV. Non-spin-flip (NSF) and spin-flip (SF) scattering plots represent the spin dynamics along the $[111]$ cubic direction and the $[h+k, -h+k, -2k]$ plane, respectively. We show in Figs. 4(c) and 4(d) the corresponding calculations for NSF and SF scattering using single tetrahedron theory. The experimental data and the single tetrahedron calculations for the NSF case are in qualitative agreement, whereas the comparison of the SF results shows a distinct difference, in particular in the low- Q range. Considering that the energy resolution for our experiment in the elastic channel was about 0.3 meV, one can argue that the experimental data capture excitations below that energy. Thus the observed difference between the single tetrahedron theory calculations and the SF experimental result could possibly be due to the weak intertetrahedron interactions. This argument would be aligned with what we discussed earlier to explain the thermodynamics results at ultralow temperatures. Further experiments with higher energy resolution and corresponding calculations are needed to confirm this theory.

In conclusion, we report evidence of $\text{Ba}_3\text{Yb}_2\text{Zn}_5\text{O}_{11}$ being an interacting quantum breathing pyrochlore spin-1/2 system, contrary to previous theoretical treatments assuming uncorrelated tetrahedra. The ultralow-temperature μ^+ SR results demonstrate persistent spin dynamics, and the thermal conductivity data, collected at the same temperature range, suggest itinerant fermionic excitations. Furthermore, the polarized inelastic neutron scattering results collected in the low-energy range appear to diverge from the previously proposed single tetrahedron model. Clearly, follow-up experiments are needed to confirm the nature of the spin interactions in $\text{Ba}_3\text{Yb}_2\text{Zn}_5\text{O}_{11}$ in the low-temperature–low-energy regime; however, based on our current experimental results we suggest

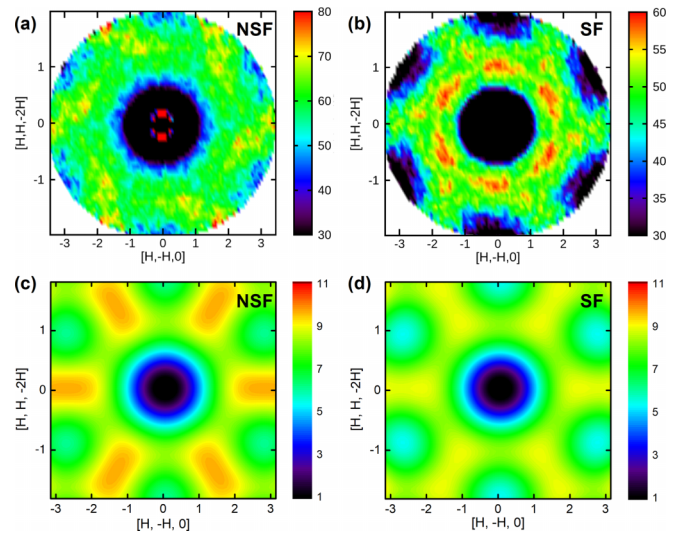


FIG. 4. (a) and (b) show the polarized neutron scattering data measured at $T = 0.1$ K and $E = 0.5$ meV, after subtracting data at $T = 50$ K and $E = 0.5$ meV as the background. (c) and (d) present the calculations of NSF and SF scattering using single tetrahedron theory outlined in the text.

that a simple effective XXZ model, formulated in terms of the lowest-energy doublets per tetrahedron, can account for the ultralow-temperature specific heat measured at low external field $\mu_0 H \lesssim 1$ T. Additionally, in this Research Letter we report that the ac-susceptibility and TDO measurements show two anomalies at $\mu_0 H = 0.32, 1.0$ T, suggesting that the system goes through two transitions yet to be understood. Our findings open the gates toward a landscape of breathing pyrochlore materials and nontrivial exotic phases of matter, including fracton physics, that can be realized within it [25–27].

We are thankful to William Steinhardt, Jeffrey Rau, and Michel Gingras for fruitful discussions. Research performed at Duke University is supported by National Science Foundation Grant No. DMR-1828348. A portion of this work was performed at the National High Magnetic Field Laboratory, which is supported by National Science Foundation

Cooperative Agreements No. DMR-1157490 and No. DMR-1644779, the State of Florida, and the U.S. Department of Energy. We acknowledge the support of EPSRC (United Kingdom) and the facilities of the Hamilton high-performance computing service of Durham University. Muon measurements were performed at the Swiss Muon Source and the STFC-ISIS facility, and we are grateful for the provision of beamtime. Access to Multi Axis Crystal Spectrometer (MACS) polarized neutron measurements was provided by the Center for High Resolution Neutron Scattering, a partnership between the National Institute of Standards and Technology and the National Science Foundation under Agreement No. DMR-1508249. A.H.N. and H.Y. were supported by National Science Foundation Grant No. DMR-1917511. S.H. acknowledges support provided by funding from the William M. Fairbank Chair in Physics at Duke University and from the Powe Junior Faculty Enhancement award.

-
- [1] *Introduction to Frustrated Magnetism: Materials, Experiments, Theory*, edited by C. Lacroix, P. Mendels, and F. Mila, Springer Series in Solid-State Sciences Vol. 164 (Springer, New York, 2011).
- [2] L. Balents, Spin liquids in frustrated magnets, *Nature (London)* **464**, 199 (2010).
- [3] M. Subramanian, G. Aravamudan, and G. Subba Rao, Oxide pyrochlores - a review, *Prog. Solid State Chem.* **15**, 55 (1983).
- [4] J. S. Gardner, M. J. P. Gingras, and J. E. Greedan, Magnetic pyrochlore oxides, *Rev. Mod. Phys.* **82**, 53 (2010).
- [5] J. G. Rau and M. J. Gingras, Frustrated quantum rare-earth pyrochlores, *Annu. Rev. Condens. Matter Phys.* **10**, 357 (2019).
- [6] A. M. Hallas, J. Gaudet, and B. D. Gaulin, Experimental insights into ground-state selection of quantum XY pyrochlores, *Annu. Rev. Condens. Matter Phys.* **9**, 105 (2018).
- [7] B. Gao, T. Chen, D. W. Tam, C.-L. Huang, K. Sasmal, D. T. Adroja, F. Ye, H. Cao, G. Sala, M. B. Stone, C. Baines, J. A. T. Verezhak, H. Hu, J.-H. Chung, X. Xu, S.-W. Cheong, M. Nallaiyan, S. Spagna, M. B. Maple, A. H. Nevidomskyy *et al.*, Experimental signatures of a three-dimensional quantum spin liquid in effective spin-1/2 $\text{Ce}_2\text{Zr}_2\text{O}_7$ pyrochlore, *Nat. Phys.* **15**, 1052 (2019).
- [8] L. Savary, K. A. Ross, B. D. Gaulin, J. P. C. Ruff, and L. Balents, Order by Quantum Disorder in $\text{Er}_2\text{Ti}_2\text{O}_7$, *Phys. Rev. Lett.* **109**, 167201 (2012).
- [9] K. Kimura, S. Nakatsuji, J. J. Wen, C. Broholm, M. B. Stone, E. Nishibori, and H. Sawa, Quantum fluctuations in spin-ice-like $\text{Pr}_2\text{Zr}_2\text{O}_7$, *Nat. Commun.* **4**, 1934 (2013).
- [10] J. Oitmaa, R. R. P. Singh, B. Javanparast, A. G. R. Day, B. V. Bagheri, and M. J. P. Gingras, Phase transition and thermal order-by-disorder in the pyrochlore antiferromagnet $\text{Er}_2\text{Ti}_2\text{O}_7$: A high-temperature series expansion study, *Phys. Rev. B* **88**, 220404(R) (2013).
- [11] S. T. Bramwell, M. J. Harris, B. C. den Hertog, M. J. P. Gingras, J. S. Gardner, D. F. McMorrow, A. R. Wildes, A. L. Cornelius, J. D. M. Champion, R. G. Melko, and T. Fennell, Spin Correlations in $\text{Ho}_2\text{Ti}_2\text{O}_7$: A Dipolar Spin Ice System, *Phys. Rev. Lett.* **87**, 047205 (2001).
- [12] A. P. Ramirez, A. Hayashi, R. J. Cava, R. Siddharthan, and B. S. Shastry, Zero-point entropy in ‘spin ice’, *Nature (London)* **399**, 333 (1999).
- [13] I. Mirebeau, I. N. Goncharenko, G. Dhalenne, and A. Revcolevschi, Pressure and Field Induced Magnetic Order in the Spin Liquid $\text{Tb}_2\text{Ti}_2\text{O}_7$ as Studied by Single Crystal Neutron Diffraction, *Phys. Rev. Lett.* **93**, 187204 (2004).
- [14] L.-J. Chang, S. Onoda, Y. Su, Y.-J. Kao, K.-D. Tsuei, Y. Yasui, K. Kakurai, and M. R. Lees, Higgs transition from a magnetic Coulomb liquid to a ferromagnet in $\text{Yb}_2\text{Ti}_2\text{O}_7$, *Nat. Commun.* **3**, 992 (2012).
- [15] M. E. Zhitomirsky, M. V. Gvozdikova, P. C. W. Holdsworth, and R. Moessner, Quantum Order by Disorder and Accidental Soft Mode in $\text{Er}_2\text{Ti}_2\text{O}_7$, *Phys. Rev. Lett.* **109**, 077204 (2012).
- [16] J. G. Rau, S. Petit, and M. J. P. Gingras, Order by virtual crystal field fluctuations in pyrochlore XY antiferromagnets, *Phys. Rev. B* **93**, 184408 (2016).
- [17] K. A. Ross, L. Savary, B. D. Gaulin, and L. Balents, Quantum Excitations in Quantum Spin Ice, *Phys. Rev. X* **1**, 021002 (2011).
- [18] N. R. Hayre, K. A. Ross, R. Applegate, T. Lin, R. R. P. Singh, B. D. Gaulin, and M. J. P. Gingras, Thermodynamic properties of $\text{Yb}_2\text{Ti}_2\text{O}_7$ pyrochlore as a function of temperature and magnetic field: Validation of a quantum spin ice exchange Hamiltonian, *Phys. Rev. B* **87**, 184423 (2013).
- [19] J. D. Thompson, P. A. McClarty, H. M. Rønnow, L. P. Regnault, A. Sørge, and M. J. P. Gingras, Rods of Neutron Scattering Intensity in $\text{Yb}_2\text{Ti}_2\text{O}_7$: Compelling Evidence for Significant Anisotropic Exchange in a Magnetic Pyrochlore Oxide, *Phys. Rev. Lett.* **106**, 187202 (2011).
- [20] L. Savary, X. Wang, H.-Y. Kee, Y. B. Kim, Y. Yu, and G. Chen, Quantum spin ice on the breathing pyrochlore lattice, *Phys. Rev. B* **94**, 075146 (2016).
- [21] F.-Y. Li, Y.-D. Li, Y. B. Kim, L. Balents, Y. Yu, and G. Chen, Weyl magnons in breathing pyrochlore antiferromagnets, *Nat. Commun.* **7**, 12691 (2016).
- [22] K. Aoyama, M. Gen, and H. Kawamura, Effects of spin-lattice coupling and a magnetic field in classical Heisenberg

- antiferromagnets on the breathing pyrochlore lattice, *Phys. Rev. B* **104**, 184411 (2021).
- [23] K. Aoyama and H. Kawamura, Hedgehog-lattice spin texture in classical Heisenberg antiferromagnets on the breathing pyrochlore lattice, *Phys. Rev. B* **103**, 014406 (2021).
- [24] M. V. Talanov and V. M. Talanov, Formation of breathing pyrochlore lattices: Structural, thermodynamic and crystal chemical aspects, *CrystEngComm* **22**, 1176 (2020).
- [25] H. Yan, O. Benton, L. D. C. Jaubert, and N. Shannon, Rank-2 $U(1)$ Spin Liquid on the Breathing Pyrochlore Lattice, *Phys. Rev. Lett.* **124**, 127203 (2020).
- [26] S. E. Han, A. S. Patri, and Y. B. Kim, Realization of fractonic quantum phases in the breathing pyrochlore lattice, *Phys. Rev. B* **105**, 235120 (2022).
- [27] L. E. Chern, Y. B. Kim, and C. Castelnovo, Competing quantum spin liquids, gauge fluctuations, and anisotropic interactions in a breathing pyrochlore lattice, *Phys. Rev. B* **106**, 134402 (2022).
- [28] M. Gen, Y. Okamoto, M. Mori, K. Takenaka, and Y. Kohama, Magnetization process of the breathing pyrochlore magnet $\text{CuInCr}_4\text{S}_8$ in ultrahigh magnetic fields up to 150 T, *Phys. Rev. B* **101**, 054434 (2020).
- [29] S. Lee, S.-H. Do, W.-J. Lee, Y. S. Choi, M. Lee, E. S. Choi, A. P. Reyes, P. L. Kuhns, A. Ozarowski, and K.-Y. Choi, Multistage symmetry breaking in the breathing pyrochlore lattice $\text{Li}(\text{Ga}, \text{In})\text{Cr}_4\text{O}_8$, *Phys. Rev. B* **93**, 174402 (2016).
- [30] Y. Okamoto, G. J. Nilsen, J. P. Attfield, and Z. Hiroi, Breathing Pyrochlore Lattice Realized in A-Site Ordered Spinel Oxides $\text{LiGaCr}_4\text{O}_8$ and $\text{LiInCr}_4\text{O}_8$, *Phys. Rev. Lett.* **110**, 097203 (2013).
- [31] Y. Okamoto, G. J. Nilsen, T. Nakazono, and Z. Hiroi, Magnetic phase diagram of the breathing pyrochlore antiferromagnet $\text{LiGa}_{1-x}\text{In}_x\text{Cr}_4\text{O}_8$, *J. Phys. Soc. Jpn.* **84**, 043707 (2015).
- [32] G. Pokharel, A. F. May, D. S. Parker, S. Calder, G. Ehlers, A. Huq, S. A. J. Kimber, H. S. Arachchige, L. Poudel, M. A. McGuire, D. Mandrus, and A. D. Christianson, Negative thermal expansion and magnetoelastic coupling in the breathing pyrochlore lattice material $\text{LiGaCr}_4\text{S}_8$, *Phys. Rev. B* **97**, 134117 (2018).
- [33] P. Ghosh, Y. Iqbal, T. Müller, R. T. Ponnaganti, R. Thomale, R. Narayanan, J. Reuther, M. J. P. Gingras, and H. O. Jeschke, Breathing chromium spinels: A showcase for a variety of pyrochlore Heisenberg Hamiltonians, *npj Quantum Mater.* **4**, 63 (2019).
- [34] S. Gao, A. F. May, M.-H. Du, J. A. M. Paddison, H. S. Arachchige, G. Pokharel, C. dela Cruz, Q. Zhang, G. Ehlers, D. S. Parker, D. G. Mandrus, M. B. Stone, and A. D. Christianson, Hierarchical excitations from correlated spin tetrahedra on the breathing pyrochlore lattice, *Phys. Rev. B* **103**, 214418 (2021).
- [35] X. Gui, E. Feng, H. Cao, and R. J. Cava, Ferromagnetic $\text{Cr}_4\text{PtGa}_{17}$: A half-Heusler-type compound with a breathing pyrochlore lattice, *J. Am. Chem. Soc.* **143**, 14342 (2021).
- [36] S. Sharma, M. Pocrnic, B. N. Richtig, C. R. Wiebe, J. Beare, J. Gautreau, J. P. Clancy, J. P. C. Ruff, M. Pula, Q. Chen, S. Yoon, Y. Cai, and G. M. Luke, Synthesis and physical and magnetic properties of $\text{CuAlCr}_4\text{S}_8$: A Cr-based breathing pyrochlore, *Phys. Rev. B* **106**, 024407 (2022).
- [37] K. Kimura, S. Nakatsuji, and T. Kimura, Experimental realization of a quantum breathing pyrochlore antiferromagnet, *Phys. Rev. B* **90**, 060414(R) (2014).
- [38] J. G. Rau, L. S. Wu, A. F. May, L. Poudel, B. Winn, V. O. Garlea, A. Huq, P. Whitfield, A. E. Taylor, M. D. Lumsden, M. J. P. Gingras, and A. D. Christianson, Anisotropic Exchange within Decoupled Tetrahedra in the Quantum Breathing Pyrochlore $\text{Ba}_3\text{Yb}_2\text{Zn}_5\text{O}_{11}$, *Phys. Rev. Lett.* **116**, 257204 (2016).
- [39] T. Haku, K. Kimura, Y. Matsumoto, M. Soda, M. Sera, D. Yu, R. A. Mole, T. Takeuchi, S. Nakatsuji, Y. Kono, T. Sakakibara, L.-J. Chang, and T. Masuda, Low-energy excitations and ground-state selection in the quantum breathing pyrochlore antiferromagnet $\text{Ba}_3\text{Yb}_2\text{Zn}_5\text{O}_{11}$, *Phys. Rev. B* **93**, 220407(R) (2016).
- [40] T. Haku, M. Soda, M. Sera, K. Kimura, S. Itoh, T. Yokoo, and T. Masuda, Crystal field excitations in the breathing pyrochlore antiferromagnet $\text{Ba}_3\text{Yb}_2\text{Zn}_5\text{O}_{11}$, *J. Phys. Soc. Jpn.* **85**, 034721 (2016).
- [41] T. Haku, M. Soda, M. Sera, K. Kimura, J. Taylor, S. Itoh, T. Yokoo, Y. Matsumoto, D. Yu, R. A. Mole, T. Takeuchi, S. Nakatsuji, Y. Kono, T. Sakakibara, L.-J. Chang, and T. Masuda, Neutron scattering study in breathing pyrochlore antiferromagnet $\text{Ba}_3\text{Yb}_2\text{Zn}_5\text{O}_{11}$, *J. Phys.: Conf. Ser.* **828**, 012018 (2017).
- [42] J. G. Rau, L. S. Wu, A. F. May, A. E. Taylor, I.-L. Liu, J. Higgins, N. P. Butch, K. A. Ross, H. S. Nair, M. D. Lumsden, M. J. P. Gingras, and A. D. Christianson, Behavior of the breathing pyrochlore lattice $\text{Ba}_3\text{Yb}_2\text{Zn}_5\text{O}_{11}$ in applied magnetic field, *J. Phys.: Condens. Matter* **30**, 455801 (2018).
- [43] S. Dissanayake, Z. Shi, J. G. Rau, R. Bag, W. Steinhardt, N. P. Butch, M. Frontzek, A. Podlesnyak, D. Graf, C. Marjerrison, J. Liu, M. J. Gingras, and S. Haravifard, Towards understanding the magnetic properties of the breathing pyrochlore compound $\text{Ba}_3\text{Yb}_2\text{Zn}_5\text{O}_{11}$ through single-crystal studies, *npj Quantum Mater.* **7**, 77 (2022).
- [44] J. Möller, P. Bonfà, D. Ceresoli, F. Bernardini, S. Blundell, T. Lancaster, R. De Renzi, N. Marzari, I. Watanabe, S. Sulaiman, and M. I. Mohamed-Ibrahim, Playing quantum hide-and-seek with the muon: Localizing muon stopping sites, *Phys. Scr.* **88**, 068510 (2013).
- [45] See Supplemental Material at <http://link.aps.org/supplemental/10.1103/PhysRevB.107.L140408> for the sample synthesis, crystal growth, measurement techniques, additional heat capacity data, and detailed theoretical effective model; this includes Refs. [17,25,26,38–40,42,54–70].
- [46] S. H. Curnoe, Quantum spin configurations in $\text{Tb}_2\text{Ti}_2\text{O}_7$, *Phys. Rev. B* **75**, 212404 (2007).
- [47] Y. Xu, J. Zhang, Y. S. Li, Y. J. Yu, X. C. Hong, Q. M. Zhang, and S. Y. Li, Absence of Magnetic Thermal Conductivity in the Quantum Spin-Liquid Candidate YbMgGaO_4 , *Phys. Rev. Lett.* **117**, 267202 (2016).
- [48] M. Sutherland, D. G. Hawthorn, R. W. Hill, F. Ronning, S. Wakimoto, H. Zhang, C. Proust, E. Boaknin, C. Lupien, L. Taillefer, R. Liang, D. A. Bonn, W. N. Hardy, R. Gagnon, N. E. Hussey, T. Kimura, M. Nohara, and H. Takagi, Thermal conductivity across the phase diagram of cuprates: Low-energy quasiparticles and doping dependence of the superconducting gap, *Phys. Rev. B* **67**, 174520 (2003).
- [49] X. Rao, G. Hussain, Q. Huang, W. J. Chu, N. Li, X. Zhao, Z. Dun, E. S. Choi, T. Asaba, L. Chen, L. Li, X. Y. Yue, N. N. Wang, J.-G. Cheng, Y. H. Gao, Y. Shen, J. Zhao, G. Chen, H. D. Zhou, and X. F. Sun, Survival of itinerant excitations and quantum spin state transitions in YbMgGaO_4 with chemical disorder, *Nat. Commun.* **12**, 4949 (2021).

- [50] S. Y. Li, J.-B. Bonnemaïson, A. Payeur, P. Fournier, C. H. Wang, X. H. Chen, and L. Taillefer, Low-temperature phonon thermal conductivity of single-crystalline Nd_2CuO_4 : Effects of sample size and surface roughness, *Phys. Rev. B* **77**, 134501 (2008).
- [51] J. M. Ni, Y. Y. Huang, E. J. Cheng, Y. J. Yu, B. L. Pan, Q. Li, L. M. Xu, Z. M. Tian, and S. Y. Li, Giant isotropic magneto-thermal conductivity of metallic spin liquid candidate $\text{Pr}_2\text{Ir}_2\text{O}_7$ with quantum criticality, *Nat. Commun.* **12**, 307 (2021).
- [52] Y. J. Yu, Y. Xu, K. J. Ran, J. M. Ni, Y. Y. Huang, J. H. Wang, J. S. Wen, and S. Y. Li, Ultralow-Temperature Thermal Conductivity of the Kitaev Honeycomb Magnet $\alpha\text{-RuCl}_3$ across the Field-Induced Phase Transition, *Phys. Rev. Lett.* **120**, 067202 (2018).
- [53] P. Bourgeois-Hope, F. Lalibert e, E. Lefran ois, G. Grissonnanche, S. R. de Cotret, R. Gordon, S. Kitou, H. Sawa, H. Cui, R. Kato, L. Taillefer, and N. Doiron-Leyraud, Thermal Conductivity of the Quantum Spin Liquid Candidate $\text{EtMe}_3\text{Sb}[\text{Pd}(\text{dmit})_2]_2$: No Evidence of Mobile Gapless Excitations, *Phys. Rev. X* **9**, 041051 (2019).
- [54] B. Huddart, A. Hern andez-Meli an, T. Hicken, M. Gomil sek, Z. Hawkhead, S. Clark, F. Pratt, and T. Lancaster, MuFinder: A program to determine and analyse muon stopping sites, *Comput. Phys. Commun.* **280**, 108488 (2022).
- [55] S. J. Clark, M. D. Segall, C. J. Pickard, P. J. Hasnip, M. I. Probert, K. Refson, and M. C. Payne, First principles methods using CASTEP, *Z. Kristallogr.* **220**, 567 (2005).
- [56] H. J. Monkhorst and J. D. Pack, Special points for Brillouin-zone integrations, *Phys. Rev. B* **13**, 5188 (1976).
- [57] F. R. Foronda, F. Lang, J. S. M oller, T. Lancaster, A. T. Boothroyd, F. L. Pratt, S. R. Giblin, D. Prabhakaran, and S. J. Blundell, Anisotropic Local Modification of Crystal Field Levels in Pr-Based Pyrochlores: A Muon-Induced Effect Modeled Using Density Functional Theory, *Phys. Rev. Lett.* **114**, 017602 (2015).
- [58] A. Keren, G. Bazalitsky, I. Campbell, and J. S. Lord, Probing exotic spin correlations by muon spin depolarization measurements with applications to spin glass dynamics, *Phys. Rev. B* **64**, 054403 (2001).
- [59] *Muon Spectroscopy*, edited by S. J. Blundell, R. De Renzi, T. Lancaster, and F. L. Pratt (Oxford University Press, Oxford, 2022).
- [60] R. B. Clover and W. P. Wolf, Magnetic susceptibility measurements with a tunnel diode oscillator, *Rev. Sci. Instrum.* **41**, 617 (1970).
- [61] C. T. Van Degrift, Tunnel diode oscillator for 0.001 ppm measurements at low temperatures, *Rev. Sci. Instrum.* **46**, 599 (1975).
- [62] Z. Shi, W. Steinhardt, D. Graf, P. Corboz, F. Weickert, N. Harrison, M. Jaime, C. Marjerrison, H. A. Dabkowska, F. Mila, and S. Haravifard, Emergent bound states and impurity pairs in chemically doped Shastry-Sutherland system, *Nat. Commun.* **10**, 2439 (2019).
- [63] J. Rodriguez, D. Adler, P. Brand, C. Broholm, J. Cook, C. Brocker, R. Hammond, Z. Huang, P. Hundertmark, J. Lynn, N. C. Maliszewskyj, J. Moyer, J. Orndorff, D. Pierce, T. D. Pike, G. Scharfstein, S. A. Smees, and R. Vilaseca, MACS—a new high intensity cold neutron spectrometer at NIST, *Meas. Sci. Technol.* **19**, 034023 (2008).
- [64] Q. Ye, T. Gentile, J. Anderson, C. Broholm, W. Chen, Z. DeLand, R. Erwin, C. Fu, J. Fuller, A. Kirchhoff, J. A. Rodriguez-Rivera, V. Thampy, T. G. Walker, and S. Watson, Wide angle polarization analysis with neutron spin filters, *Phys. Procedia* **42**, 206 (2013).
- [65] C. Fu, T. R. Gentile, G. L. Jones, W. Chen, R. Erwin, S. Watson, C. Broholm, J. Rodriguez-Rivera, and J. Scherschligt, A wide angle neutron spin filter system using polarized ^3He , *Phys. B (Amsterdam)* **406**, 2419 (2011).
- [66] W. Chen, T. R. Gentile, Q. Ye, A. Kirchhoff, S. Watson, J. Rodriguez-Rivera, Y. Qiu, and C. Broholm, Recent advancements of wide-angle polarization analysis with ^3He neutron spin filters, in *VI European Conference on Neutron Scattering (ECNS2015) 30 August to 4 September 2015, Zaragoza, Spain, Journal of Physics: Conference Series* Vol. 746 (Institute of Physics, London, 2016), p. 012016.
- [67] R. Moon, T. Riste, and W. Koehler, Polarization analysis of thermal-neutron scattering, *Phys. Rev.* **181**, 920 (1969).
- [68] K. Lefmann and C. Rischel, Quantum effects in magnetic structures on the fcc lattice, *Eur. Phys. J. C* **21**, 313 (2001).
- [69] M. S. Seehra and T. M. Giebultowicz, Magnetic structures of fcc systems with nearest-neighbor and next-nearest-neighbor exchange interactions, *Phys. Rev. B* **38**, 11898 (1988).
- [70] A. M. Cook, S. Matern, C. Hickey, A. A. Aczel, and A. Paramakanti, Spin-orbit coupled $j_{\text{eff}} = 1/2$ iridium moments on the geometrically frustrated fcc lattice, *Phys. Rev. B* **92**, 020417(R) (2015).